

Quantum entanglement correlations in double quark PDFs

Adrian Dumitru* and Eric Kolbusz†

Department of Natural Sciences, Baruch College, CUNY,
17 Lexington Avenue, New York, NY 10010, USA and

The Graduate School and University Center, The City University of New York, 365 Fifth Avenue, New York, NY 10016, USA

Methods from Quantum Information Theory are used to scrutinize quantum correlations encoded in the two-quark density matrix over light-cone momentum fractions x_1 and x_2 . A non-perturbative three quark model light-cone wavefunction predicts significant non-classical correlations associated with the “entanglement negativity” measure for asymmetric and small quark momentum fractions. We perform one step of QCD scale evolution of the entire density matrix, not just its diagonal (dPDF), by computing collinearly divergent corrections due to the emission of a gluon. Finally, we present first qualitative numerical results for single-step scale evolution of quantum entanglement correlations in double quark PDFs. At a higher Q^2 scale, the non-classical correlations manifest in the dPDF for nearly symmetric momentum fractions.

CONTENTS

I. Introduction	1
A. Detection of Quantum Correlations	3
II. Double Quark Parton Distribution for the Three Quark Fock State	4
A. The Three Quark Fock State	4
B. Purging Entanglement Negativity with the PEN transformation	5
C. Leveraging Center of Mass Variables	5
D. Numerical Results for the Quark dPDF	6
III. Evolution to Higher Scales	9
A. Corrections to the density matrix due to one gluon emission	9
B. Cancellation of Soft Divergence	12
C. DGLAP evolution of the diagonal of the density matrix	13
D. Numerical Results	14
IV. Summary	14
V. Acknowledgements	16
References	16

I. INTRODUCTION

Multi parton interactions (MPI) may occur in high energy proton-proton or proton-nucleus collisions whereby two or more partons from the projectile proton undergo a hard scattering off the target. The simplest such MPI process corresponds to double parton scattering which involves double parton distributions (dPDFs) [1–4]; we refer to ref. [5] for a review of the theory of double parton scattering. A setup for the computation of double parton distributions via lattice QCD has been described in ref. [6]. dPDFs describe the joint distribution of two partons with light-cone (LC) momentum fractions x_1 and x_2 , respectively, in the proton.

dPDFs provide very interesting insight into parton *correlations* in the proton. Indeed, a number of authors have concluded that a simple factorized dPDF, lacking correlations when $x_1 + x_2 < 1$, of the form

$$f_{ij}(x_1, x_2, Q^2) = f_i(x_1, Q^2) f_j(x_2, Q^2) \Theta(1 - x_1 - x_2) \quad (1)$$

* adrian.dumitru@baruch.cuny.edu

† ekolbusz@gradcenter.cuny.edu

does not provide a good approximation to the full dPDF [1–3, 7, 8]. Here, i and j denote parton flavors, and it has been assumed that the MPI involve a single hard scale Q^2 , for simplicity. We shall first consider the double quark PDF at a low virtuality Q_0^2 of order a hadronic scale; henceforth Q_0^2 will be omitted from the arguments of the dPDFs. If the dPDF at the initial scale Q_0^2 lacks correlations, then factorization of the dPDF is preserved by QCD evolution. In sec. III we perform a single evolution step towards higher Q^2 of the entire density matrix including its off-diagonal elements¹. This provides first qualitative insight into double parton quantum correlations encoded in the density matrix at $Q^2 > Q_0^2$.

A variety of initial conditions for dPDFs with correlations have been proposed. The model by Gaunt and Sterling (GS) [2] for the valence quark dPDFs corresponds to

$$f_{ij}(x_1, x_2) = f_i(x_1) f_j(x_2) \frac{(1 - x_1 - x_2)^2}{(1 - x_1)^{2+n} (1 - x_2)^{2+n}} \quad (2)$$

with $n = 0.5$. It is understood that the support of this function is restricted to $x_1, x_2 > 0$ and $x_1 + x_2 \leq 1$. In this model correlations arise mainly due to the phase space restriction and the dPDF approaches a factorized form as $x_1 + x_2 \ll 1$.

Another model (“model II” in [7]) for correlated valence quark dPDFs has been proposed by Broniowski and Arriola (BA)

$$f_{ij}(x_1, x_2) = f_i(x_1) f_j(x_2) \frac{725}{28} \frac{(x_1 + x_2)^2}{(1 - x_1)(1 + 6x_1 + 16x_1^2 + 6x_1^3 + x_1^4)(1 - x_2)(1 + 6x_2 + 16x_2^2 + 6x_2^3 + x_2^4)} \quad (3)$$

This model respects the quark number and momentum sum rules. However, here $f_{ij}(x_1, x_2)/f_i(x_1) f_j(x_2)$ does not vanish as $x_1 + x_2 \rightarrow 1$.

In passing we mention also ref. [10] who proposed a construction of initial conditions (at a low Q^2 scale) for double gluon PDFs from single gluon PDFs. Here we focus on quark dPDFs.

Valence double quark PDFs have also been computed in a “bag model” of the proton [11]. In a “rigid bag” approximation the dPDF factorizes and there are no correlations. However, other treatments of the bag do break factorization into single quark PDFs. In the bag model we do not have a simple analytic form of the dPDF like in the two models mentioned above, and so we will not consider it further in this paper. We do note, however, that this model in principle does provide the complete two-quark density matrix including its off-diagonal elements. Hence, it may be possible to distinguish quantum vs. classical correlations using methods similar to those employed here.

Rinaldi *et al.* have derived double quark distributions from a constituent quark model light-cone wavefunction (LCwf) of the proton [12–14] by “tracing over” the remaining quark. This way, all sum rules are satisfied by construction. A rather similar approach is presented here. However, our formulation also provides the *off-diagonal* elements of the two-quark density matrix. While not required for the construction of the dPDF, knowledge of the entire density matrix is needed to determine the nature of correlations, such as quantum vs. classical, by the application of methods from Quantum Information Theory (QIT).

While the present focus is on double quark PDFs as a function of LC momentum fraction, we note that “flavor interference dPDFs” have recently been mentioned in the literature [15]. These correspond to off-diagonal elements of the two-quark density matrix over flavor, analogous to the off-diagonal elements of the two-quark density matrix over x considered here. As already mentioned above, the novel aspect here is to show how specific methods from QIT can be employed to scrutinize the classical vs. quantum nature of double quark correlations.

There has been great interest recently in understanding various aspects of entanglement of quarks and gluons in the proton, initiated primarily by the work of Kharzeev *et al.* [16–18] as well as Kovner *et al.* [9, 19–22]. Ref. [23], which focuses on the rapidity evolution of the entanglement entropy, provides a list of additional references on this topic. Moreover, Hatta *et al.* have recently analyzed entanglement of spin and orbital angular momentum degrees of freedom [24, 25].

The goal of this paper is to explore the application of QIT methods to reveal the potential presence of quantum correlations in double quark PDFs. In the following sec. IA we identify a measure for quantum correlations and a method for suppressing them in order to study the effect on the dPDF. In sec. II we introduce a simple, non-perturbative constituent quark model for the effective light-cone wave function of the proton which provides us with the entire two-quark density matrix including off-diagonal elements. Furthermore, we identify a valid “partitioning” of the reduced density matrix, in terms of unconstrained variables for the quark momentum fractions, in order to be able to study subsystem correlations with QIT methods. We discuss the convergence of the eigenspace of the

¹ We note in passing that ref. [9] considered small- x evolution, in the high gluon density limit, of the complete density matrix for soft gluons.

discretized, partially transposed density matrix towards an infinite dimensional null space times a finite dimensional subspace for non-zero eigenvalues. Sec. III is devoted to the implementation of the first step of perturbative QCD scale evolution of the *entire* two-quark density matrix. Only the diagonal elements evolve in terms of convolutions of splitting functions with dPDFs but such treatment is insufficient for an analysis of the scale evolution of quantum correlations.

A. Detection of Quantum Correlations

Our goal is to identify specific correlations in the two-quark density matrix (and hence, the dPDF) which cannot arise classically and therefore must be quantum in nature. General information theoretical analysis of correlations is basis-independent and so requires the eigenvalues of the density matrix, meaning that knowledge of the entire matrix, not just its diagonal, is necessary. We will briefly summarize the relevant QIT theory for the sake of completeness.

Given two systems (e.g. quark 1 and quark 2) separately described by density matrices ρ^A and ρ^B in Hilbert spaces \mathcal{H}^A and \mathcal{H}^B , there are multiple possibilities for the behavior of the combined system. If the subsystems are disjoint, then the total density matrix $\rho = \rho^A \otimes \rho^B$ is called a product state and clearly has no correlations between the two systems. In the case of two quarks, this corresponds to a factorized dPDF as in (1), however without the kinematic constraint that $x_1 + x_2 \leq 1$.

To introduce correlations, we have to create a mixed state as some weighted sum over product states, as the GS and BA dPDFs do in (2) and (3). A special case is a state that can be written as a classical probability distribution over product states

$$\rho^{AB} = \sum_i p_i \rho_i^A \otimes \rho_i^B \quad (4)$$

with $\sum p_i = 1$, called a separable state. These states exhibit correlations between the two subsystems, but the correlations can be entirely explained classically². Note that the subsystems can be quantum in nature—we are only commenting on the relationships between them. On the other hand, a state which is not separable must have correlations due to quantum entanglement.

Identifying whether or not a given density matrix is separable is known to be NP-hard [26, 27], so there is no known universal test. However, many partial methods [28–30] have been formulated for use on specific subsets of density matrices.

One standard measure of entanglement is the entanglement entropy [31]. Given a pure bipartite system ρ^{AB} over $\mathcal{H}^A \otimes \mathcal{H}^B$, we can form a reduced density matrix ρ^A by only tracing over \mathcal{H}^B . The (von Neumann) entanglement entropy is then defined as

$$S_{\text{vN}}(\rho^A) = -\text{tr}(\rho^A \log \rho^A) . \quad (5)$$

This definition is symmetric over A and B ; tracing over \mathcal{H}^A and calculating $S_{\text{vN}}(\rho_B)$ instead will yield the same value. If $S_{\text{vN}}(\rho_A) > 0$, we conclude that the two subsystems are entangled. In the next section we start from a pure state describing the proton, but then immediately perform a partial trace over all but two degrees of freedom (d.o.f.) to obtain a mixed state $\rho_{x_1 x_2, x'_1 x'_2}$ with $S_{\text{vN}} > 0$. Since our two-quark density matrix is already mixed, we cannot use the entanglement entropy to draw conclusions about the nature of correlations between the LC momentum fractions of the quarks.

Another operation we can perform on the bipartite density matrix ρ^{AB} is to transpose only one of the subsystems ρ^B ; this is called the partial transpose and is written ρ^{T_B} . The Peres-Horodecki criterion [32, 33] states that if this partial transpose has any negative eigenvalues, it cannot be separable, and hence must exhibit some quantum correlations. The absolute value of the sum of these negative eigenvalues is called the negativity $\mathcal{N}(\rho)$. This is a partial result since the inverse of the criterion, that $\mathcal{N}(\rho) = 0$ implies that ρ is separable, is only true when $\dim(\mathcal{H}^A \otimes \mathcal{H}^B)$ is either 2×2 or 2×3 .

Many other computable quantities, such as the coherent information [34], exist to study quantum correlations between subsystems. Nevertheless, we shall rely on the Peres-Horodecki criterion and entanglement negativity in our analysis of double quark PDFs in the proton. In fact, we are mostly interested not in quantifying the overall “degree of entanglement correlations” but rather in investigating how such correlations affect the dPDF. In this regard, working with the partially transposed density matrix is useful because its negative eigenvalues can be “purged” to construct a nearby density matrix with negativity zero from which the corresponding dPDF follows. This is the idea we pursue in the next section.

² This state can easily be prepared using LOCC: use a classical random number generator to choose outcome i with probability p_i , then locally prepare state $\rho_i^A \otimes \rho_i^B$ based on the outcome.

II. DOUBLE QUARK PARTON DISTRIBUTION FOR THE THREE QUARK FOCK STATE

A. The Three Quark Fock State

The proton state $|P\rangle$ can be written as a coherent superposition of all possible Fock states multiplied by their respective Fock space amplitudes, the light-cone wavefunctions. For moderate momentum fractions $x_i \sim 0.1$ and transverse momenta $|\vec{k}_i| \sim \Lambda_{\text{QCD}}$, the three valence quark state should dominate and we approximate the light-cone state of the proton by an effective three-quark wavefunction:

$$|P\rangle = |P^+, P_\perp = 0\rangle = \int_{[0,1]^3} [dx_i] \int [d^2 k_i] \Psi_{\text{qqq}}(k_1, k_2, k_3) |k_1; k_2; k_3\rangle \quad (6)$$

where

$$[dx_i] = \prod_{i=1\cdots 3} \frac{dx_i}{2x_i} \delta\left(1 - \sum_i x_i\right), \quad [d^2 k_i] = \prod_{i=1\cdots 3} \frac{d^2 k_i}{(2\pi)^3} (2\pi)^3 \delta\left(\sum_i \vec{k}_i\right), \quad (7)$$

and $k_i = (x_i P^+, \vec{k}_i)$ are the three-momenta of the constituent quarks. The spatial wavefunction is symmetric under exchange of any two quarks, $\Psi_{\text{qqq}}(k_1, k_2, k_3) = \Psi_{\text{qqq}}(k_2, k_1, k_3)$ etc. Since our focus is on correlations in momentum space, we will always trace out spin-flavor and color d.o.f. and assume that eq. (6) provides an effective description of the state in momentum space.

To construct the corresponding density matrix we choose basis states of the form

$$|\alpha\rangle = \frac{1}{16\pi^3} \frac{|x_1, \vec{k}_1; x_2, \vec{k}_2; x_3, \vec{k}_3\rangle}{\sqrt{x_1 x_2 x_3}} \rightarrow \langle P|\alpha\rangle = \frac{\Psi_{\text{qqq}}^*(x_i, \vec{k}_i)}{2\sqrt{x_1 x_2 x_3}} \delta\left(1 - \sum x_i\right) \delta\left(\sum \vec{k}_i\right). \quad (8)$$

The density matrix for the proton state is then

$$\rho_{\alpha\alpha'} = \frac{\Psi_{\text{qqq}}^*(x'_i, \vec{k}'_i)}{2\sqrt{x'_1 x'_2 x'_3}} \frac{\Psi_{\text{qqq}}(x_i, \vec{k}_i)}{2\sqrt{x_1 x_2 x_3}}, \quad (9)$$

where the matrix “indices” are $\alpha = \{x_1, \vec{k}_1, x_2, \vec{k}_2\}$, $\alpha' = \{x'_1, \vec{k}'_1, x'_2, \vec{k}'_2\}$; it is implied that the r.h.s. is evaluated for $x_3 = 1 - x_1 - x_2$ and $\vec{k}_3 = -\vec{k}_1 - \vec{k}_2$ (and similar for the primed variables). The trace of the density matrix is computed as

$$\text{tr } \rho = \int dx_1 dx_2 \int \frac{d^2 k_1}{16\pi^3} \frac{d^2 k_2}{16\pi^3} \rho_{\alpha\alpha} = 2 \int [dx_i] \frac{1}{4} \int [d^2 k_i] \left| \Psi_{\text{qqq}}(x_i, \vec{k}_i) \right|^2. \quad (10)$$

We can then construct the reduced density matrix for x_1 and x_2 by tracing over the remaining degrees of freedom, given by an integral over the quark transverse momenta

$$\rho_{x_1 x_2, x'_1 x'_2} = \frac{1}{4} \int [d^2 k_i] \rho_{\alpha\alpha'} . \quad (11)$$

This reduced density matrix, which has non-zero entropy, will be evaluated in sec. II C below.

To date the exact light-cone wavefunction of the proton is unknown, of course, as it requires solving the QCD Hamiltonian. Here we employ a simple model due to Brodsky and Schlumpf (BS) [35, 36] where we take

$$\Psi_{\text{qqq}} = N \sqrt{x_1 x_2 x_3} e^{-\mathcal{M}^2/2\beta^2}, \quad (12)$$

with $\mathcal{M}^2 = \sum (\vec{k}_i^2 + m_q^2)/x_i$ being the invariant mass squared of the non-interacting three quark system [37]. The parameters $m_q = 0.26$ GeV and $\beta = 0.55$ GeV have been tuned in refs. [35, 36] to reproduce various properties of the proton such as its electromagnetic form factors. The normalization factor N of the LCwf is determined from $\text{tr } \rho = 1$.

More involved approaches consider various model Hamiltonians with interactions, and possibly higher Fock states such as $|qqqg\rangle$ or $|qqqq\bar{q}\rangle$, and the quark model LCwf are then obtained numerically. Ref. [38] has recently studied quark and gluon entanglement in the proton in this way. However, the wavefunctions and density matrices are then available only numerically. For this first exploration of quantum correlations associated with the entanglement negativity measure we consider the simple BS model above.

B. Purging Entanglement Negativity with the PEN transformation

The PEN (Purge Entanglement Negativity) algorithm, introduced and detailed in ref. [39], can be used to remove the negativity of a density matrix. Namely, it takes a density matrix ρ and produces a new density matrix ρ' such that $\mathcal{N}(\rho') = 0$ by replacing all negative eigenvalues of ρ^{T_2} with zeroes³. In short, after diagonalizing ρ^{T_2} the negative eigenvalues are replaced by 0; we then undo the unitary transformation to the eigenbasis of ρ^{T_2} and the partial transposition, and finally rescale the matrix by $1/(1 + \mathcal{N}(\rho))$ so that $\text{tr } \rho' = 1$. Note that ρ' is not guaranteed to be separable, except for small Hilbert spaces where the Peres-Horodecki criterion is sufficient to establish separability. However, since the negative eigenvalues of the partial transpose of ρ are necessarily associated with quantum correlations, these specific correlations must be removed when the associated eigenvalue is sent to zero.

In some low-dimensional cases such as Bell states⁴, where ρ^{T_2} features a single non-degenerate negative eigenvalue, ρ' is the closest separable state to ρ , i.e. a separable Werner state [40]. If ρ is separable to begin with then the PEN transformation reduces to the identity and $\rho' = \rho$.

C. Leveraging Center of Mass Variables

In this section we construct the reduced density matrix for the LC momentum fraction degrees of freedom of two quarks. The transverse momentum integrals over the BS wavefunction in eq. (11) can be done by hand, yielding

$$\rho_{x_1 x_2, x'_1 x'_2} \sim \frac{\exp\left[-\frac{m_q^2}{2\beta^2}(A_1 + A_2 + A_3)\right]}{A_1 A_2 + A_1 A_3 + A_2 A_3} \quad (13)$$

with $A_i = \frac{1}{x_i} + \frac{1}{x'_i}$. Recall that x_3 is not an independent variable, and should be read as shorthand for $1 - x_1 - x_2$ (likewise for x'_3). We now have a mixed density matrix with two subsystems for the two valence quark LC momentum fractions.

The denominator $A_1 A_2 + A_1 A_3 + A_2 A_3$ does not seem readily factorizable into a polynomial in x_1 times a polynomial in x_2 on the diagonal, suggesting that this is not a classical dPDF i.e. it cannot be written as a classical mixture of product states. Our goal is to confirm this guess by numerically exhibiting the presence of quantum correlations in the dPDF. If we go about this the naive way, using the PEN algorithm to erase the negativity of $\rho_{x_1 x_2, x'_1 x'_2}$, the resulting density matrix does not respect the kinematic $x_1 + x_2 \leq 1$ constraint of the problem and gives an unphysical dDPF. The simple reason for this is that given $x_1 + x_2 \leq 1$ and $x'_1 + x'_2 \leq 1$, partial transposition (swapping x_2 and x'_2) does not necessarily respect these constraints.

The solution is to use center-of-mass (c.o.m.) coordinates that decouple relative and c.o.m. motion, and factorize the constraints of the problem [37]. By finding the dPDF in the c.o.m. variables, using the PEN algorithm on the c.o.m. density matrix, then changing back to our original variables x_1 and x_2 , we remove negativity while preserving the momentum constraint.

A set of suitable relative light-cone coordinates for three particles constrained to $x_1 + x_2 + x_3 = 1$ is [37]

$$\xi = \frac{x_1}{x_1 + x_2} , \quad \eta = x_1 + x_2 , \quad (14)$$

with $\xi, \eta \in [0, 1]$. In terms of these variables,

$$2[\text{d}x_i] \frac{1}{4}[\text{d}^2 k_i] = \frac{\text{d}\xi \text{d}\eta}{2\xi(1-\xi)2\eta(1-\eta)} \frac{1}{4}[\text{d}^2 k_i] , \quad (15)$$

and

$$\rho_{\xi\eta, \xi'\eta'} = \frac{1}{4} \int [\text{d}^2 k_i] \frac{\Psi_{\text{qqq}}^*(\xi'\eta', \eta'(1-\xi'), 1-\eta', \vec{k}_1, \vec{k}_2, \vec{k}_3)}{\sqrt{4\eta'(1-\eta')\xi'(1-\xi')}} \frac{\Psi_{\text{qqq}}(\xi\eta, \eta(1-\xi), 1-\eta, \vec{k}_1, \vec{k}_2, \vec{k}_3)}{\sqrt{4\eta(1-\eta)\xi(1-\xi)}} \quad (16)$$

is the reduced density matrix over the remaining ξ, η degrees of freedom. It is normalized such that

$$1 = \int \text{d}\xi \text{d}\eta \rho_{\xi\eta, \xi\eta} . \quad (17)$$

³ The resulting ρ' is, indeed, a valid density matrix in that it has unit trace, and is hermitian and positive semi-definite.

⁴ A different example is given in appendix B of ref. [39]. There, a $N_C^2 \times N_C^2$ dimensional anti-symmetric color space state is considered where ρ^{T_2} also exhibits a single negative, and a fully degenerate spectrum of positive eigenvalues. It is shown that the application of PEN results in the minimal admixture of the identity so as to achieve a separable Werner state.

So far ξ and η are continuous variables on $[0, 1]$. In order to evaluate $\rho_{\xi\eta, \xi'\eta'}$ on a computer and analyze it with information theoretical techniques, we need a finite dimensional matrix. This is achieved by discretizing the unit interval into a finite number of bins of size $\Delta\xi$ and $\Delta\eta$. The discretized density matrix is

$$\tilde{\rho}_{\xi\eta, \xi'\eta'} = \Delta\xi \Delta\eta \rho_{\xi\eta, \xi'\eta'} . \quad (18)$$

We can then construct the partial transpose $\tilde{\rho}^{T_2}$ and numerically calculate the negativity. For the BS light-cone wavefunction, we employed $\Delta\xi = \Delta\eta$ bins of width $\frac{1}{N}$ for $N = 20, 40, 80, 160$ and found that $\mathcal{N}(\tilde{\rho}_{\xi\eta, \xi'\eta'})$ converges to ~ 0.035 . This is because once the variation of $\tilde{\rho}^{T_2}$ across a bin is small a further decrease of the bin width only increases the dimension of the null space of the matrix. That is, as the number N of bins increases, the eigenvalue density of $\tilde{\rho}^{T_2}$ asymptotically approaches the form

$$\frac{dN_\lambda}{d\lambda} = \left((N+1)^2 - \sum_{i=1}^n C_i \right) \delta(\lambda) + \sum_{i=1}^n C_i \delta(\lambda - \lambda_i) \quad (19)$$

where C_i is the multiplicity of the nonzero eigenvalue λ_i . This can be seen in fig. 1. There are $N_\lambda = (N+1)^2$ total eigenvalues of the partial transpose, but all but a few of them remain in a delta function peak at zero. The nonzero eigenvalues do not drift as N changes, so increasing N only increases the resolution for these values. One notable nonzero eigenvalue is -0.03 which provides most of the contribution to the negativity of $\tilde{\rho}$.

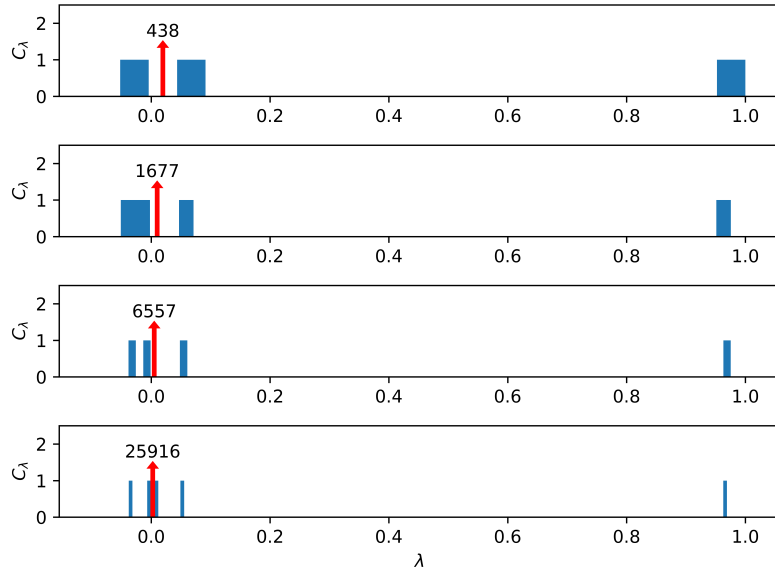


FIG. 1: Eigenvalue spectrum of the partial transpose $\tilde{\rho}^{T_2}$ for $\frac{1}{\Delta\xi} = \frac{1}{\Delta\eta} = 20, 40, 80, 160$. The red arrows at the origin signify $\delta(\lambda)$ peaks in the continuum limit. We have chosen to show these peaks as arrows labeled with their correct height, rather than plotting these peaks and obscuring the nonzero eigenvalues.

Once we use the PEN algorithm to purge the negative eigenvalues of the partial transpose, we can return to (discrete) x_1 - x_2 space for example, to compute single and double PDFs as functions of x_1, x_2 as described below.

For the BS light-cone wavefunction, we find the negativity of $\rho_{\xi\eta, \xi'\eta'}$ to be ~ 0.035 . This may be interpreted in the sense that quantum correlations are weak. However, we already mentioned at the end of sec. IA that we are mostly interested not in the overall (averaged over momentum fractions) “degree of entanglement”, but in how the presence of quantum correlations affects the dPDF. In the following section we shall see that purging the negativity of the density matrix can result in substantial modification of the dPDF, at least in specific regions of x_1 - x_2 space.

D. Numerical Results for the Quark dPDF

We can compare the structure of the dPDF, both pre- and post-PEN, to models such as the GS model (2) and the BA model (3) by plotting the ratio of the dPDF to the product of two single-quark PDFs,

$$C(x_1, x_2) = \frac{f_{qq}(x_1, x_2)}{f_q(x_1) f_q(x_2)} . \quad (20)$$

If the dPDF is simply a product of two single-quark PDFs without any correlations, then this ratio is 1. The dPDF is given by the diagonal elements of the reduced density matrix defined above in eqs. (9, 11),

$$f_{qq}(x_1, x_2) = \rho_{x_1 x_2, x_1 x_2} . \quad (21)$$

This relation can be confirmed by direct computation of the matrix element in the proton state (6) of the operator

$$\frac{\pi P^+}{(2\pi)^3} \int d^2z \int dz_1^- dz_2^- dz_3^- e^{-ix_2 P^+(z_1^- - z_2^-) - ix_1 P^+ z_3^-} O(z_1^- + \vec{z}, z_2^- + \vec{z}) O(z_3^-, 0) \quad (22)$$

with $O(z, y) = \bar{q}(z)\gamma^+ q(y)$, and $q(z)$ the quark field operator at point z . (The notation $z^- + \vec{z}$ refers to a vector with LC minus component z^- , and transverse components \vec{z} which represent the transverse spatial separation of the quarks.) In sec. III C below we verify that $f_{qq}(x_1, x_2)$ satisfies the dPDF Dokshitzer-Gribov-Lipatov-Altarelli-Parisi (DGLAP) equation upon emission of a collinear gluon.

The single quark PDF is given by⁵ the integral of the dPDF over x_2 from 0 to $1 - x_1$,

$$f_q(x_1) = \int_0^{1-x_1} dx_2 f_{qq}(x_1, x_2) . \quad (23)$$

The dPDF momentum sum rule [2] is satisfied⁶ thanks to $f_{qq}(x_1, x_2) = f_{qq}(x_1, 1 - x_1 - x_2)$. We also confirm that $3 \int dx_1 x_1 f_q(x_1) = 2 \int [dx_i] (x_1 + x_2 + x_3) \frac{1}{4} \int [d^2 k_i] |\Psi_{\text{qqq}}(x_1, x_2, x_3, \vec{k}_1, \vec{k}_2, \vec{k}_3)|^2 = \text{tr } \rho = 1$.

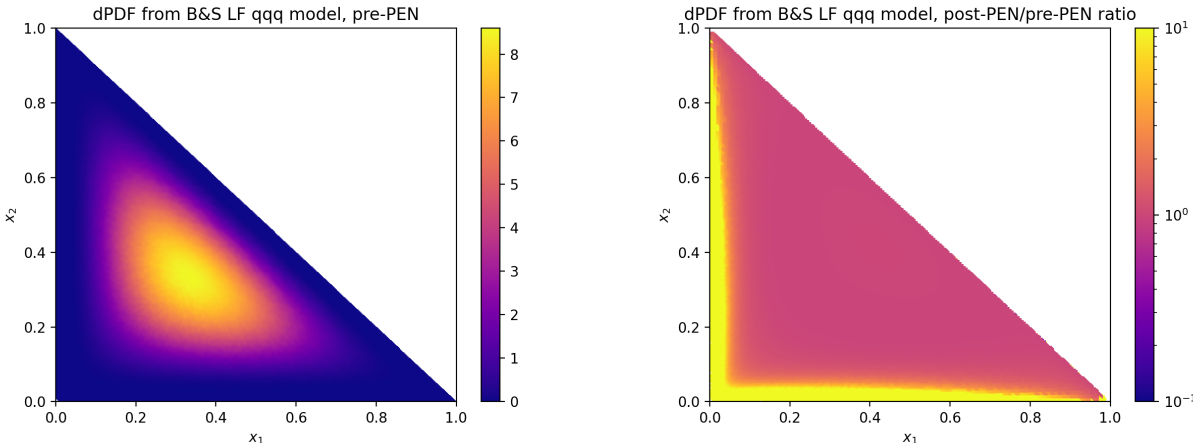


FIG. 2: Left: the double quark PDF of the LC quark model (see text) in the x_1 - x_2 plane. Right: the ratio of the double quark PDF after removal of the entanglement negativity to the original dPDF shown on the left.

In fig. 2(left) we show the double quark PDF $f_{qq}(x_1, x_2)$ of the LC quark model described in sec. II A. As expected, it peaks around $x_1 \sim x_2 \sim 1/3$ with tails extending to smaller x_i . The panel on the right shows the dPDF after removal of the entanglement negativity of the density matrix (via the PEN transformation), divided by the original dPDF. In much of the allowed range of x_1, x_2 the PEN transformation has affected the dPDF by a factor of order 1, hence PEN is close to the identity map over a large portion of the domain. For x_1 or x_2 less than approximately 0.1 the dPDF has changed by a factor of 10 or more. Of course, in the region of small x_i , and for Q^2 greater than the confinement scale, one expects sea partons to dominate. In sec. III below we shall study the effects on the quark dPDF due to the perturbative emission of a gluon.

Our main interest is in the nature of correlations encoded in the dPDF. Hence, in fig. 3 we plot the correlation factor $C(x_1, x_2)$, eq. (20), as a function of x_1 for various x_2 . For small $x_2 = 0.14$, the GS model predicts weak correlations up to $x_1 \approx 0.5$ which then turn into an anti-correlation as the boundary of phase space is approached. The correlation measure obtained from the BS wavefunction is close to the BA model for a large portion of phase

⁵ Eq. (23) can be confirmed by computing the Dirac electromagnetic form factor which in the limit of vanishing momentum transfer reduces to $\int dx f_q(x) = F_1(0) = 1$.

⁶ That is,

$$\int dx_2 x_2 f_{qq}(x_1, x_2) + \int dx_3 x_3 f_{qq}(x_1, x_3) = (1 - x_1) f_q(x_1) .$$

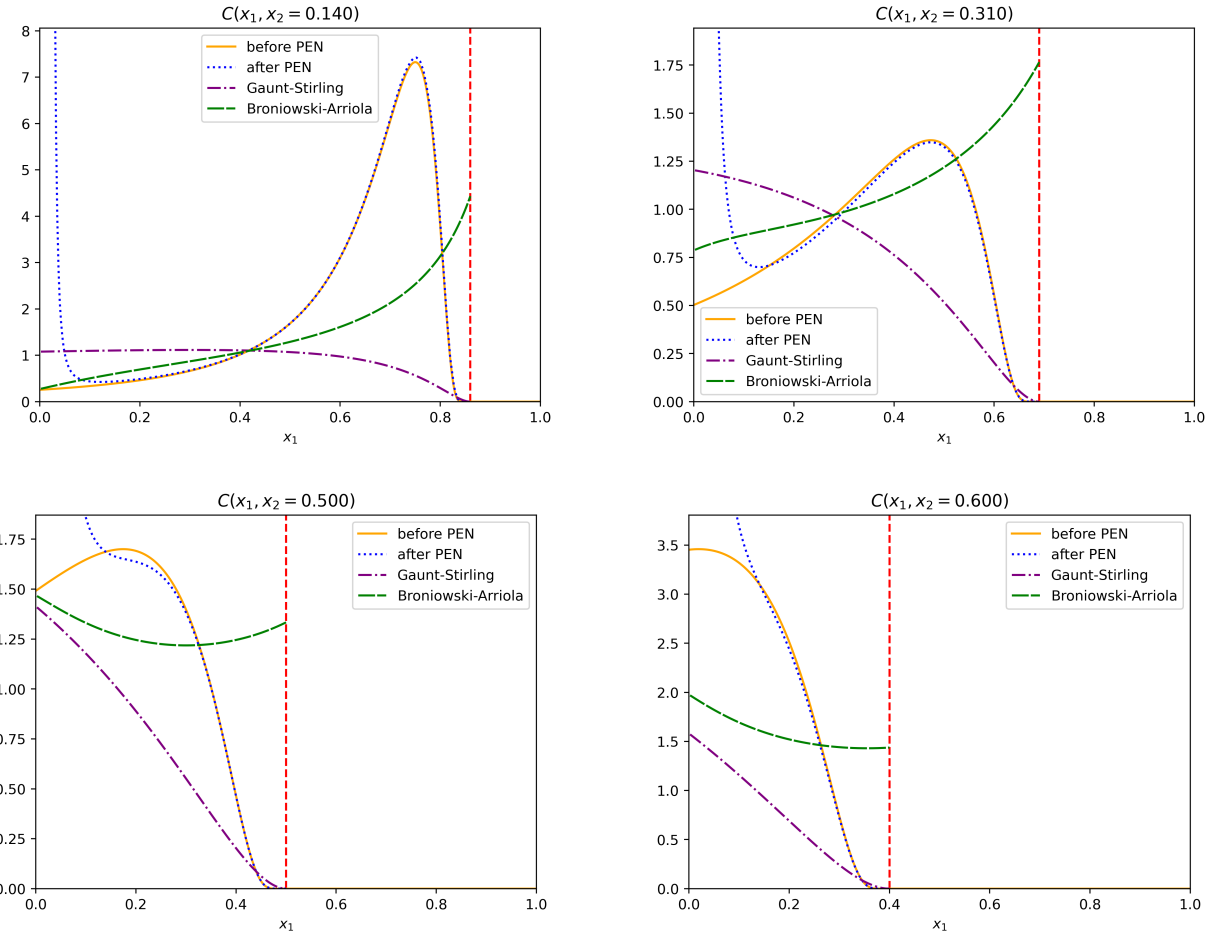


FIG. 3: Some selected slices of constant x_2 for the ratio of the dPDF to the product of two PDFs. The vertical dashed line represents the kinematic boundary where $x_1 + x_2 = 1$. The dash-dotted and dashed curves correspond to the GS [2] and BA [7] models given in eqs. (2,3), respectively. The solid and dotted curves refer to the dPDF obtained here from the Brodsky-Schlumpf model LCwf [35, 36] before and after the removal of quantum correlations via the PEN algorithm.

space from $x_1 \sim 0.05$ to ~ 0.5 ; the anti-correlation at small x_1 , $C(x_1, x_2) < 1$, weakens with increasing x_1 . The BS wavefunction predicts a much stronger correlation for large $x_1 \simeq 0.7$ but this extreme part of phase space is less relevant in practice. *Removal* of the quantum correlations associated with negativity (by application of PEN) does not affect the dPDF much when $x_1 \gtrsim 0.1$ but it does lead to a strong correlation peak at small $x_1 < 0.1$. Hence, assuming that the GS, BA, and the BS LCwf models are close to the real dPDF of QCD we conclude that the LC quark model wavefunction requires the presence of subsystem quantum correlations so as not to strongly overpredict the dPDF at small x_2 , and yet smaller $x_1 < x_2$.

For $x_2 \simeq 0.3$ we still see fair agreement between the dPDF from the BS wavefunction and the BA model from $x_1 \sim 0.1$ to ~ 0.5 . Here, the two qualitatively differ from the GS curve which shows a monotonic decrease and a suppressed dPDF at $x_1 \geq 0.3$. However, the LC quark model and the GS model both predict a strong suppression of the dPDF towards the edge of phase space, unlike the BA model. We also again observe the appearance of a strong enhancement of the dPDF of the LC quark model at small $x_1 \leq 0.1$ when the quantum correlations (associated with the negativity measure) of the two quark density matrix are removed.

For the panels in the first row of fig. 3 we may identify the following structure in the BS model. There exists a *quantum correlated* regime at small $x_1 < x_q^*$ where the positive slope of $C(x_1, x_2)$ is due to quantum correlations; this regime extends up to about $x_q^* \approx 0.1\text{--}0.15$ where the dotted and solid lines merge. Beyond x_q^* , correlations are classical as the dotted and solid lines are on top of each other. However, we can subdivide this further into a *classically correlated* regime up to x_c^* , which is the point where the curves reach their maximum. In the classically correlated regime between x_q^* and x_c^* , $C(x_1, x_2)$ again exhibits a positive slope. Lastly, beyond x_c^* we have the *cutoff* regime where the dPDF drops to 0 very rapidly, faster than the sPDF $f_q(x_1)$, and the slope of $C(x_1, x_2)$ is negative. This arises due to the increasing importance of the momentum constraint.

Proceeding to greater $x_2 = 0.5$ we again observe a strong enhancement of the dPDF at small $x_1 \lesssim 0.2$ due to PEN. This *quantum correlated* regime then transitions right away into the *cutoff* regime, i.e. the intermediate *classically correlated* regime for $x_q^* < x_1 < x_c^*$ has been “squeezed out” by the merging *quantum correlated* and *cutoff* regimes.

For $x_2 = 0.6$, the pre- and post-PEN curves exhibit similar behavior. Small phase space suppresses quantum correlations in that both curves exhibit a downward trend. However, the presence of quantum correlations again prevents a stronger enhancement of the dPDF below $x_1 \sim 0.1$. This is maintained as x_2 heads towards the upper extreme of phase space.

Summarizing this section, we find that for rather asymmetric momentum fractions x_1 and x_2 , and well below the kinematic boundary $x_1 + x_2 = 1$, the BS model LCwf does exhibit significant quantum correlations associated with the negativity measure. On the other hand, for $x_1 \simeq x_2$ or large $x_1 + x_2$, while the dPDF can be substantially different from the product of single quark PDFs, nevertheless these correlations are not associated with entanglement negativity.

III. EVOLUTION TO HIGHER SCALES

So far we have considered the correlations of the dPDF at a low resolution scale Q_0^2 where a LC quark model may apply. Naturally, one may be interested in how Fig. 3 changes as we evolve to higher scales. The DGLAP evolution of dPDFs to high Q^2 has been studied extensively in the literature, see e.g. [1–5, 7, 8, 10]. However, analysis of classical vs. quantum correlations using negativity and PEN requires knowledge of the entire density matrix, not just the diagonal elements, so we must evolve the entire density matrix. Hence, we require an extension of the dPDF DGLAP equations to off-diagonal density matrix elements. Here we consider only the first step of scale evolution where one of the three valence quarks splits into a quark and a gluon. We consider diagrams which exhibit a collinear divergence. In this section we will use expressions derived in sec. 3 of [41], and in [42] where the quark wavefunction renormalization factor (virtual corrections) and the Fock space amplitude in the LC gauge of the $|qqqg\rangle$ state (real emissions) have been determined.

A. Corrections to the density matrix due to one gluon emission

Depending on where we insert our basis states, $\rho_{\alpha\alpha'} = \langle P|\alpha\rangle\langle\alpha'|P\rangle$, in fig. 4, we have to consider either a gluon emitted and absorbed by the same quark in $|P\rangle$ or $\langle P|$, i.e. a virtual correction, or a “real emission” diagram where a gluon is exchanged by quark i in $|P\rangle$ and the corresponding quark in $\langle P|$.

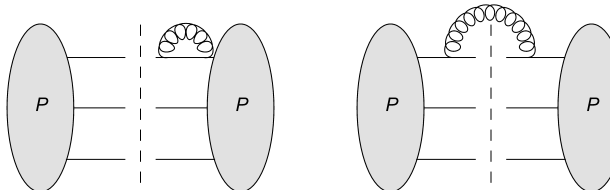


FIG. 4: Two diagrams representing, respectively, the emission and absorption of a gluon by quark 1, and the exchange of a gluon between quarks 1' and 1. The dashed line represents the insertion of two-quark basis states.

There are six diagrams of the first type and three of the second type.

The first case gives the quark wavefunction renormalization factor $Z_q^{1/2} = (1 - C_q)^{1/2} \simeq 1 - C_q/2$ via

$$C_q \left(x_i; x, \frac{M_{\text{UV}}}{m_{\text{col}}} \right) = \frac{2g^2 C_F N_C}{3} \int_x^1 \frac{dx_g}{x_g} \int \frac{d^2 k_g}{16\pi^3} \Theta(x_i - x_g) \left[1 + (1 - z)^2 \right] \left[\frac{1}{k_g^2 + \Delta^2} - \frac{1}{k_g^2 + \Lambda^2} \right] \quad (24)$$

$$= \frac{\alpha_s}{\pi} C_F \log \frac{M_{\text{UV}}^2}{m_{\text{col}}^2} \left[\log \frac{x_i}{x} - \frac{(3x_i - x)(x_i - x)}{4x_i^2} \right] \Theta(x_i - x) . \quad (25)$$

Here $z = x_g/x_i$, and $\Delta = zm_{\text{col}}$ where m_{col} denotes a quark mass regulator for the collinear singularity. $N_C = 3$ the number of colors in QCD, $C_F = (N_C^2 - 1)/2N_C = 4/3$ the quadratic Casimir of the fundamental representation, and $\alpha_s = g^2/4\pi$ the coupling. The factor $C_F[1 + (1 - z)^2]$ represents, of course, the splitting function $zP_{g \leftarrow q}(z)$.

We have regularized the UV divergence by introducing a cutoff with $\Lambda = zM_{\text{UV}}$, and the soft divergence by a cutoff x on the LC momentum fraction of the gluon. The above expression corresponds to the first step of evolution taking us from the scale m_{col} to M_{UV} . Since we consider just one single collinear gluon emission we must require that $C_q(x_i) \ll 1$.

The wavefunction renormalization factor arises for each of the six quark lines:

$$\begin{aligned} \Psi_{\text{qqq}}^*(\xi', \eta', \vec{k}'_i) \Psi_{\text{qqq}}(\xi, \eta, \vec{k}_i) \rightarrow \Psi_{\text{qqq}}^*(\xi', \eta', \vec{k}'_i) \Psi_{\text{qqq}}(\xi, \eta, \vec{k}_i) & \left[1 - \frac{1}{2} C_q \left(x_1; x, \frac{M_{\text{UV}}}{m_{\text{col}}} \right) - \frac{1}{2} C_q \left(x'_1; x, \frac{M_{\text{UV}}}{m_{\text{col}}} \right) \right. \\ & - \frac{1}{2} C_q \left(x_2; x, \frac{M_{\text{UV}}}{m_{\text{col}}} \right) - \frac{1}{2} C_q \left(x'_2; x, \frac{M_{\text{UV}}}{m_{\text{col}}} \right) \\ & \left. - \frac{1}{2} C_q \left(x_3; x, \frac{M_{\text{UV}}}{m_{\text{col}}} \right) - \frac{1}{2} C_q \left(x'_3; x, \frac{M_{\text{UV}}}{m_{\text{col}}} \right) \right] . \end{aligned} \quad (26)$$

Here the x_i should be read as shorthands for the associated expressions in terms of ξ and η as defined in (14), i.e. $x_1 = \xi\eta$, $x_2 = \eta(1 - \xi)$, and $x_3 = 1 - \eta$. For clarity from now on we shall write the arguments of the three-quark wavefunction in the following order: $\Psi_{\text{qqq}}(x_1, x_2, \vec{k}_1, \vec{k}_2)$. It is understood that the third LC momentum fraction and transverse momentum is determined by conservation of momentum.

Tracing over the quark transverse momenta \vec{k}_i then gives e.g.

$$\rho_{x_1 x_2, x'_1 x'_2}^{(11)} = -\frac{g^2 C_F}{(4\pi)^2} \log \frac{M_{\text{UV}}^2}{m_{\text{col}}^2} \frac{1}{4} \int [d^2 k_i] \int_x^1 \frac{dx_g}{x_g} \Theta(x_1 - x_g) \left[1 + (1 - z)^2 \right] \frac{\Psi_{\text{qqq}}^*(x'_1, x'_2, \vec{k}_1, \vec{k}_2)}{2\sqrt{x'_1 x'_2 x'_3}} \frac{\Psi_{\text{qqq}}(x_1, x_2, \vec{k}_1, \vec{k}_2)}{2\sqrt{x_1 x_2 x_3}} \quad (27)$$

$$= -\frac{g^2 C_F}{(4\pi)^2} \log \frac{M_{\text{UV}}^2}{m_{\text{col}}^2} \int_x^1 \frac{dx_g}{x_g} \Theta(x_1 - x_g) \left[1 + (1 - z)^2 \right] \rho_{x_1 x_2, x'_1 x'_2}^{\text{qqq}} . \quad (28)$$

$\rho_{x_1 x_2, x'_1 x'_2}^{\text{qqq}}$ is the non-perturbative reduced density matrix of the three quark state before gluon emission, see sec. II. The trace of this density matrix is computed by setting $x_1 = x'_1$, $x_2 = x'_2$ and integrating with the measure $dx_1 dx_2$, as already mentioned in eq. (10). Changing to unconstrained ξ, η variables,

$$\begin{aligned} \rho_{\xi\eta, \xi'\eta'}^{(11)} = -\frac{g^2 C_F}{(4\pi)^2} \log \frac{M_{\text{UV}}^2}{m_{\text{col}}^2} \frac{1}{4} \int [d^2 k_i] \int_x^1 \frac{dx_g}{x_g} \Theta(\xi\eta - x_g) \left[1 + (1 - z)^2 \right] \\ \frac{\Psi_{\text{qqq}}^*(\xi'\eta', \eta'(1 - \xi'), \vec{k}_1, \vec{k}_2)}{\sqrt{4\eta'(1 - \eta')\xi'(1 - \xi')}} \frac{\Psi_{\text{qqq}}(\xi\eta, \eta(1 - \xi), \vec{k}_1, \vec{k}_2)}{\sqrt{4\eta(1 - \eta)\xi(1 - \xi)}} . \end{aligned} \quad (29)$$

The trace of this density matrix is computed by setting $\xi = \xi'$, $\eta = \eta'$ and integrating with the measure $d\xi d\eta$, cf. eqs. (15,17). Adding this contribution to $\rho_{\xi\eta, \xi'\eta'}$ on the r.h.s. of eq. (16) accounts for the $\mathcal{O}(\alpha_s \log M_{\text{UV}}^2 / m_{\text{col}}^2)$ virtual correction.

Now we consider the real emission correction between quarks i and i' . The four particle density matrix for the 1 to 1' gluon exchange (summed over gluon polarizations) is

$$\begin{aligned} \rho_{\text{qqqg}}^{(11')} = \frac{g^2}{3} \sum_{m, m'} \epsilon_{m' n'_2 n'_3} (t^{a'})_{m' n'_1} \epsilon_{m n_2 n_3} (t^a)_{n_1 m} \Theta(x_1 - x_g) \Theta(x'_1 - x'_g) \\ \times \frac{\vec{n} \cdot \vec{n}'}{(n^2 + \Delta^2)(n'^2 + \Delta'^2)} (2 - z - z' + zz') \frac{\Psi_{\text{qqq}}^*(x'_1, x'_2, \vec{k}'_1, \vec{k}'_2)}{2\sqrt{x'_1 x'_2 x'_3}} \frac{\Psi_{\text{qqq}}(x_1, x_2, \vec{k}_1, \vec{k}_2)}{2\sqrt{x_1 x_2 x_3}} \end{aligned} \quad (30)$$

with $z = x_g/x_1$, Δ defined as before, $\vec{n} = \vec{k}_g - z\vec{k}_1$, and the primed variables defined analogously. Here we have used the Hilbert space basis introduced in eq. (8).

We need x_1 to refer to the daughter quark LC momentum when we project onto basis states, so we shift $x_1 \mapsto x_1 + x_g$. Doing this, then tracing over the gluon color and momentum as well as over the parent quark transverse momenta, yields

$$\begin{aligned} \rho_{x_1 x_2, x'_1 x'_2}^{(11')} = 2g^2 C_F \frac{1}{4} \int [d^2 k_i] \int_x^1 \frac{dx_g}{x_g} \Theta(1 - x_1 - x_2 - x_g) \Theta(1 - x'_1 - x'_2 - x_g) \int \frac{d^2 k_g}{16\pi^3} \\ \times \frac{\vec{n} \cdot \vec{n}'}{(n^2 + \Delta^2)(n'^2 + \Delta'^2)} (2 - z - z' + zz') \frac{\Psi_{\text{qqq}}^*(x'_1 + x_g, x'_2, \vec{k}_1, \vec{k}_2)}{2\sqrt{(x'_1 + x_g)x'_2 x'_3}} \frac{\Psi_{\text{qqq}}(x_1 + x_g, x_2, \vec{k}_1, \vec{k}_2)}{2\sqrt{(x_1 + x_g)x_2 x_3}} , \end{aligned} \quad (31)$$

where now $z = x_g/(x_1 + x_g)$, $z' = x_g/(x'_1 + x_g)$ due to the shifted arguments, and $x_3 = 1 - x_1 - x_2 - x_g$ (and similar for x'_3).

We then introduce the c.o.m. variables ξ and η in the same way as in (14) noting that now $x_3 = 1 - \eta - x_g$ and $\eta < 1 - x_g$. Furthermore,

$$\frac{dx_1 dx_2 dx_3}{4(x_1 + x_g)x_2 x_3} \delta(1 - x_1 - x_2 - x_3 - x_g) = \frac{d\xi}{2\xi(1 - \xi)} \frac{d\eta}{2\eta(1 - \eta)} \frac{\Theta(1 - \eta - x_g)}{\left(1 + \frac{x_g}{\xi\eta}\right) \left(1 - \frac{x_g}{1 - \eta}\right)} \quad (32)$$

so that

$$\begin{aligned} \rho_{\xi\eta, \xi'\eta'}^{(11')} &= 2g^2 C_F \frac{1}{4} \int [d^2 k_i] \int_x^1 \frac{dx_g}{x_g} \frac{\Theta(1 - \eta - x_g)}{\sqrt{\left(1 + \frac{x_g}{\xi\eta}\right) \left(1 - \frac{x_g}{1 - \eta}\right)}} \frac{\Theta(1 - \eta' - x_g)}{\sqrt{\left(1 + \frac{x_g}{\xi'\eta'}\right) \left(1 - \frac{x_g}{1 - \eta'}\right)}} \int \frac{d^2 k_g}{16\pi^3} \frac{\vec{n} \cdot \vec{n}'}{(n^2 + \Delta^2)(n'^2 + \Delta'^2)} \\ &\quad \times (2 - z - z' + zz') \frac{\Psi_{\text{qqq}}^*(\xi'\eta' + x_g, \eta'(1 - \xi'), \vec{k}_1, \vec{k}_2)}{\sqrt{4\eta'(1 - \eta')\xi'(1 - \xi')}} \frac{\Psi_{\text{qqq}}(\xi\eta + x_g, \eta(1 - \xi), \vec{k}_1, \vec{k}_2)}{\sqrt{4\eta(1 - \eta)\xi(1 - \xi)}} \end{aligned} \quad (33)$$

with $z = x_g/(\xi\eta + x_g)$, $z' = x_g/(\xi'\eta' + x_g)$. We verify that for $(\xi, \eta) \in (0, 1)^2$ the arguments of the three-quark wavefunctions do not take unphysical values: $x_g < 1 - \eta$ implies $\xi\eta + x_g < (\xi - 1)\eta + 1 < 1$.

The previous expression is logarithmically UV divergent and we again introduce a UV regulator as

$$\begin{aligned} &- g^2 C_F \frac{1}{4} \int [d^2 k_i] \int_x^1 \frac{dx_g}{x_g} \frac{\Theta(1 - \eta - x_g)}{\sqrt{\left(1 + \frac{x_g}{\xi\eta}\right) \left(1 - \frac{x_g}{1 - \eta}\right)}} \frac{\Theta(1 - \eta' - x_g)}{\sqrt{\left(1 + \frac{x_g}{\xi'\eta'}\right) \left(1 - \frac{x_g}{1 - \eta'}\right)}} \int \frac{d^2 k_g}{16\pi^3} (2 - z - z' + zz') \\ &\quad \times \left[\frac{1}{n^2 + \Lambda^2} + \frac{1}{n'^2 + \Lambda'^2} \right] \frac{\Psi_{\text{qqq}}^*(\xi'\eta' + x_g, \eta'(1 - \xi'), \vec{k}_1, \vec{k}_2)}{\sqrt{4\eta'(1 - \eta')\xi'(1 - \xi')}} \frac{\Psi_{\text{qqq}}(\xi\eta + x_g, \eta(1 - \xi), \vec{k}_1, \vec{k}_2)}{\sqrt{4\eta(1 - \eta)\xi(1 - \xi)}}. \end{aligned} \quad (34)$$

All together we have

$$\begin{aligned} \rho_{\xi\eta, \xi'\eta'}^{(11')} &= 2g^2 C_F \frac{1}{4} \int [d^2 k_i] \int_x^1 \frac{dx_g}{x_g} \frac{\Theta(1 - \eta - x_g)}{\sqrt{\left(1 + \frac{x_g}{\xi\eta}\right) \left(1 - \frac{x_g}{1 - \eta}\right)}} \frac{\Theta(1 - \eta' - x_g)}{\sqrt{\left(1 + \frac{x_g}{\xi'\eta'}\right) \left(1 - \frac{x_g}{1 - \eta'}\right)}} (2 - z - z' + zz') \int \frac{d^2 k_g}{16\pi^3} \\ &\quad \times \left[\frac{\vec{n} \cdot \vec{n}'}{(n^2 + \Delta^2)(n'^2 + \Delta'^2)} - \frac{1}{2} \frac{1}{n^2 + \Lambda^2} - \frac{1}{2} \frac{1}{n'^2 + \Lambda'^2} \right] \frac{\Psi_{\text{qqq}}^*(\xi'\eta' + x_g, \eta'(1 - \xi'), \vec{k}_1, \vec{k}_2)}{\sqrt{4\eta'(1 - \eta')\xi'(1 - \xi')}} \frac{\Psi_{\text{qqq}}(\xi\eta + x_g, \eta(1 - \xi), \vec{k}_1, \vec{k}_2)}{\sqrt{4\eta(1 - \eta)\xi(1 - \xi)}} \end{aligned} \quad (35)$$

At this point we pause to verify not only that the trace of the density matrix is independent of the collinear and UV (m_{col} , M_{UV}) and soft (x) cutoffs but, in fact, that the $\mathcal{O}(\alpha_s)$ correction cancels altogether so as to preserve the normalization $\text{tr } \rho = 1$.

To compute the trace of (35) we set $\xi' = \xi$, $\eta' = \eta$, and integrate over $d\xi d\eta$. We can then proceed in two ways. First, we can use eq. (32) in reverse thereby also replacing $\xi\eta \rightarrow x_1$, $\eta(1 - \xi) \rightarrow x_2$, implying $1 - \eta - x_g \rightarrow x_3$. We then undo the shift of x_1 by letting $x_1 \rightarrow x_1 - x_g$ which also introduces a $\Theta(x_1 - x_g)$ function. The resulting expression cancels (at leading logarithmic accuracy, up to power corrections) the trace of $\rho^{(11)}$ from eq. (28) plus the same contribution from the trace of $\rho^{(1'1')}$.

Alternatively, we can also verify the cancellation of the integrals for $\text{tr } \rho^{(11')} + \text{tr } \rho^{(11)} + \text{tr } \rho^{(1'1')}$ in the ξ, η variables. In $\text{tr } \rho^{(11')}$ we perform the transformation

$$\tilde{\eta} = \eta + x_g, \quad \tilde{\xi} = \frac{\xi\eta + x_g}{\eta + x_g} \quad (36)$$

so that $1 - \eta - x_g = 1 - \tilde{\eta}$, $\eta(1 - \xi) = \tilde{\eta}(1 - \tilde{\xi})$, and $\xi\eta + x_g = \tilde{\xi}\tilde{\eta}$ (similar for the primed variables). This gives rise to a factor $\Theta(\tilde{\xi}\tilde{\eta} - x_g)$, which allows us to extend the range of both $\tilde{\xi}$ and $\tilde{\eta}$ to $[0, 1]$, and restores $z = x_g/\tilde{\xi}\tilde{\eta}$ as well as $\Psi_{\text{qqq}}(\xi\eta + x_g, \eta(1 - \xi), \vec{k}_1, \vec{k}_2) = \Psi_{\text{qqq}}(\tilde{\xi}\tilde{\eta}, \tilde{\eta}(1 - \tilde{\xi}), \vec{k}_1, \vec{k}_2)$. Furthermore,

$$\frac{d\eta d\xi}{2\xi(1 - \xi) 2\eta(1 - \eta)} \frac{1}{\left(1 + \frac{x_g}{\xi\eta}\right) \left(1 - \frac{x_g}{1 - \eta}\right)} = \frac{d\tilde{\eta} d\tilde{\xi}}{2\tilde{\xi}(1 - \tilde{\xi}) 2\tilde{\eta}(1 - \tilde{\eta})} \quad (37)$$

Thus, we again obtain that the trace of eq. (35) cancels against $\text{tr } \rho^{(11)}$ (plus the same contribution from $\text{tr } \rho^{(1'1')}$).

We now continue our computation with the contribution from the 2 to 2' gluon exchange. Here we shift $x_2 \rightarrow x_2 + x_g$ so that x_2 now corresponds to the LC momentum fraction of daughter quark 2. The measure changes as

$$\frac{dx_1 dx_2 dx_3}{4x_1(x_2 + x_g)x_3} \delta(1 - x_1 - x_2 - x_3 - x_g) = \frac{d\xi}{2\xi(1 - \xi)} \frac{d\eta}{2\eta(1 - \eta)} \frac{\Theta(1 - \eta - x_g)}{\left(1 + \frac{x_g}{(1 - \xi)\eta}\right) \left(1 - \frac{x_g}{1 - \eta}\right)} . \quad (38)$$

Then

$$\begin{aligned} \rho_{\xi\eta,\xi'\eta'}^{(22')} &= 2g^2 C_F \frac{1}{4} \int [d^2 k_i] \int_x^1 \frac{dx_g}{x_g} \int \frac{d^2 k_g}{16\pi^3} \frac{\Theta(1 - \eta - x_g)}{\sqrt{\left(1 + \frac{x_g}{(1 - \xi)\eta}\right) \left(1 - \frac{x_g}{1 - \eta}\right)}} \frac{\Theta(1 - \eta' - x_g)}{\sqrt{\left(1 + \frac{x_g}{(1 - \xi')\eta'}\right) \left(1 - \frac{x_g}{1 - \eta'}\right)}} (2 - z - z' + zz') \\ &\times \left[\frac{\vec{n} \cdot \vec{n}'}{(n^2 + \Delta^2)(n'^2 + \Delta'^2)} - \frac{1}{2} \frac{1}{n^2 + \Lambda^2} - \frac{1}{2} \frac{1}{n'^2 + \Lambda'^2} \right] \frac{\Psi_{\text{qqq}}^*(\xi'\eta', \eta'(1 - \xi') + x_g, \vec{k}_1, \vec{k}_2)}{\sqrt{4\eta'(1 - \eta')\xi'(1 - \xi')}} \frac{\Psi_{\text{qqq}}(\xi\eta, \eta(1 - \xi) + x_g, \vec{k}_1, \vec{k}_2)}{\sqrt{4\eta(1 - \eta)\xi(1 - \xi)}} , \end{aligned} \quad (39)$$

where now $z = x_g/(\eta(1 - \xi) + x_g)$, $z' = x_g/(\eta'(1 - \xi') + x_g)$, $\vec{n} = \vec{k}_g - z\vec{k}_2$, and Δ, Λ and the corresponding primed variables defined as before. For this contribution the transformation

$$\tilde{\eta} = \eta + x_g , \quad \tilde{\xi} = \frac{\xi\eta}{\eta + x_g} , \quad (40)$$

which corresponds to $\tilde{\xi}\tilde{\eta} = \xi\eta$, $\tilde{\eta}(1 - \tilde{\xi}) = \eta(1 - \xi) + x_g$, is useful for checking the cancellation of the perturbative correction to the trace.

Finally, for the gluon exchange from 3 to 3', no shift from parent to daughter quark LC momentum is needed as we are interested in the reduced density matrix over quarks 1 and 2. The density matrix for this diagram is

$$\begin{aligned} \rho_{\xi\eta,\xi'\eta'}^{(33')} &= 2g^2 C_F \frac{1}{4} \int [d^2 k_i] \int_x^1 \frac{dx_g}{x_g} \int \frac{d^2 k_g}{16\pi^3} \Theta(1 - \eta - x_g) \Theta(1 - \eta' - x_g) (2 - z - z' + zz') \\ &\times \left[\frac{\vec{n} \cdot \vec{n}'}{(n^2 + \Delta^2)(n'^2 + \Delta'^2)} - \frac{1}{2} \frac{1}{n^2 + \Lambda^2} - \frac{1}{2} \frac{1}{n'^2 + \Lambda'^2} \right] \frac{\Psi_{\text{qqq}}^*(\xi'\eta', \eta'(1 - \xi'), \vec{k}_1, \vec{k}_2)}{\sqrt{4\eta'(1 - \eta')\xi'(1 - \xi')}} \frac{\Psi_{\text{qqq}}(\xi\eta, \eta(1 - \xi), \vec{k}_1, \vec{k}_2)}{\sqrt{4\eta(1 - \eta)\xi(1 - \xi)}} , \end{aligned} \quad (41)$$

with $z = x_g/(1 - \eta)$, $z' = x_g/(1 - \eta')$. Here the cancellation of the trace against the last line in (26) is seen immediately.

In summary, single step evolution of the three-quark density matrix from the scale $m_{\text{col}}^2 = Q_0^2$ to the higher scale $M_{\text{UV}}^2 = Q^2$ is performed by replacing $\Psi_{\text{qqq}}^*(\xi'\eta', \eta'(1 - \xi'), \vec{k}_1, \vec{k}_2) \Psi_{\text{qqq}}(\xi\eta, \eta(1 - \xi), \vec{k}_1, \vec{k}_2)$ in (16) by the sum of virtual corrections (26) followed by adding the density matrices (35, 39, 41) for real emissions. Our result applies in the leading log $M_{\text{UV}}/m_{\text{col}} \gg 1$ approximation when the coupling α_s is sufficiently small, and perhaps the cutoff x on the LC momentum fraction of the gluon is sufficiently large, so that the $\mathcal{O}(\alpha_s)$ contribution to the wavefunction renormalization factor (25) is small.

B. Cancellation of Soft Divergence

In the previous section, we had to introduce a cutoff x on the LC momentum of the gluon to handle the soft divergence. Here we show that this divergence cancels at leading logarithmic accuracy in the sum of real emissions and virtual corrections. Hence, the integration over x_g could in principle extend to 0.

The expressions from the previous section simplify greatly when x_g is much less than the typical momentum fraction of a quark, $\langle x_q \rangle$. We then have $z, z' \ll 1$. The integral over the gluon transverse momentum \vec{k}_g for the virtual correction in eq. (29) becomes

$$\int \frac{d^2 k_g}{16\pi^3} \left(\frac{1}{k_g^2 + \Delta^2} - \frac{1}{k_g^2 + \Lambda^2} \right) = \frac{1}{(4\pi)^2} \log \frac{M_{\text{UV}}^2}{m_{\text{col}}^2} . \quad (42)$$

For the real exchanges, the softness of the gluon implies that the daughter quark momentum is the same as that of the parent quark. Since $z, z' \ll 1$, we have $\vec{n} = \vec{n}' = \vec{k}_g$ and the integral over the gluon transverse momentum in

$\rho^{(11')}$ from eq. (35) becomes

$$2 \int \frac{d^2 k_g}{16\pi^3} \left[\frac{k_g^2}{(k_g^2 + \Delta^2)(k_g^2 + \Delta'^2)} - \frac{1}{2} \frac{1}{k_g^2 + \Lambda^2} - \frac{1}{2} \frac{1}{k_g^2 + \Lambda'^2} \right]. \quad (43)$$

Consider now the sum of the gluon exchange between quarks 1 and $1'$ plus the corresponding virtual corrections in the small x_g limit:

$$\int \frac{d^2 k_g}{16\pi^3} \left[2 \left(\frac{k_g^2}{(k_g^2 + \Delta^2)(k_g^2 + \Delta'^2)} - \frac{1}{2} \frac{1}{k_g^2 + \Lambda^2} - \frac{1}{2} \frac{1}{k_g^2 + \Lambda'^2} \right) - \left(\frac{1}{k_g^2 + \Delta^2} - \frac{1}{k_g^2 + \Lambda^2} \right) - \left(\frac{1}{k_g^2 + \Delta'^2} - \frac{1}{k_g^2 + \Lambda'^2} \right) \right]. \quad (44)$$

Note that

$$\frac{2k_g^2}{(k_g^2 + \Delta^2)(k_g^2 + \Delta'^2)} = \frac{1}{k_g^2 + \Delta^2} + \frac{1}{k_g^2 + \Delta'^2} + \frac{\Delta^2 + \Delta'^2}{2(k_g^2 + \Delta^2)(k_g^2 + \Delta'^2)}. \quad (45)$$

The last term does not contribute to the leading-log approximation and can be dropped. This results in a cancellation of the bracketed terms in (44), hence we can take $x \rightarrow 0$ with no overall soft divergence when considering the sum of these diagrams. No trace over ξ or η has been performed here: this cancellation occurs for the entire density matrix, not just the diagonal elements. The calculation is identical for quarks 2 and $2'$, and 3 and $3'$.

C. DGLAP evolution of the diagonal of the density matrix

In this section we obtain expressions for the derivative with respect to $Q^2 = M_{\text{UV}}^2$ of the diagonal elements of the density matrix, i.e. the double quark PDF. These can be expressed in terms of convolutions of splitting functions and dPDFs.

We have from eq. (28), using relations (9,11),

$$Q^2 \frac{\partial}{\partial Q^2} \rho_{x_1 x_2, x_1 x_2}^{(11)} = Q^2 \frac{\partial}{\partial Q^2} \rho_{x_1 x_2, x_1 x_2}^{(1'1')} = -\frac{\alpha_s}{4\pi} \int_{x/x_1}^1 dz P_{g \leftarrow q}(z) \rho_{x_1 x_2, x_1 x_2}^{\text{qqq}}. \quad (46)$$

$\rho_{x_1 x_2, x'_1 x'_2}^{\text{qqq}}$ denotes the non-perturbative reduced density matrix obtained from the three quark LCwf before gluon emission, see sec. II. Similarly,

$$Q^2 \frac{\partial}{\partial Q^2} \rho_{x_1 x_2, x_1 x_2}^{(22)} = Q^2 \frac{\partial}{\partial Q^2} \rho_{x_1 x_2, x_1 x_2}^{(2'2')} = -\frac{\alpha_s}{4\pi} \int_{x/x_2}^1 dz P_{g \leftarrow q}(z) \rho_{x_1 x_2, x_1 x_2}^{\text{qqq}}, \quad (47)$$

$$Q^2 \frac{\partial}{\partial Q^2} \rho_{x_1 x_2, x_1 x_2}^{(33)} = Q^2 \frac{\partial}{\partial Q^2} \rho_{x_1 x_2, x_1 x_2}^{(3'3')} = -\frac{\alpha_s}{4\pi} \int_{\frac{x}{1-x_1-x_2}}^1 dz P_{g \leftarrow q}(z) \rho_{x_1 x_2, x_1 x_2}^{\text{qqq}}. \quad (48)$$

Continuing with the real emission corrections,

$$Q^2 \frac{\partial}{\partial Q^2} \rho_{x_1 x_2, x_1 x_2}^{(11')} = \frac{2\alpha_s}{4\pi} \int_{x_1/(1-x_2)}^{x_1/(x_1+x)} \frac{dz}{z} P_{g \leftarrow q}(1-z) \rho_{\frac{x_1}{z} x_2, \frac{x_1}{z} x_2}^{\text{qqq}}, \quad (49)$$

$$Q^2 \frac{\partial}{\partial Q^2} \rho_{x_1 x_2, x_1 x_2}^{(22')} = \frac{2\alpha_s}{4\pi} \int_{x_2/(1-x_1)}^{x_2/(x_2+x)} \frac{dz}{z} P_{g \leftarrow q}(1-z) \rho_{x_1 \frac{x_2}{z}, x_1 \frac{x_2}{z}}^{\text{qqq}}, \quad (50)$$

$$Q^2 \frac{\partial}{\partial Q^2} \rho_{x_1 x_2, x_1 x_2}^{(33')} = \frac{2\alpha_s}{4\pi} \int_{\frac{x}{1-x_1-x_2}}^1 dz P_{g \leftarrow q}(z) \rho_{x_1 x_2, x_1 x_2}^{\text{qqq}}. \quad (51)$$

The last term simply cancels the corresponding virtual corrections.

The expressions above reproduce the standard equations for DGLAP evolution of double quark PDFs⁷ with the identification $f_{qq}(x_1, x_2) = \rho_{x_1 x_2, x_1 x_2}$, which agrees with eq. (21). The standard form of the dPDF DGLAP equations is

$$\partial_t f_{qq}(x_1, x_2) = \int_0^{1-x_2} du K(x_1, u) f_{qq}(u, x_2) + \int_0^{1-x_1} du K(x_2, u) f_{qq}(x_1, u) , \quad (52)$$

where $t = \log Q^2$. For example, the contribution involving the real emission kernel

$$K_R(x, u) = \frac{\alpha_s}{2\pi} \frac{1}{u} P_{qq}(x/u) \Theta(u - x) \quad (53)$$

corresponds exactly to the sum of (49, 50). To see this, use the relation $P_{gq}(1-z) = P_{qq}(z)$ and the transformation $u = x_1/z$ or $u = x_2/z$, and finally send the cutoff $x \rightarrow 0$. The virtual corrections serve to ensure conservation of probability.

Hence, the diagonal of the density matrix evolves according to dPDF DGLAP via a convolution with splitting functions, and independently of the off-diagonal elements.

D. Numerical Results

In this section we present first qualitative results on the evolution of quantum correlations in the dPDF to higher scales by evaluating the correction to the density matrix due to the emission of one collinear gluon. The full evolution equation would sum multiple parton splitting steps, a more involved task which we defer to future work.

To keep the perturbative correction small we employ an unrealistically small coupling, $\alpha_s = 0.1$, and a fairly large cutoff $x = 0.1$ on the LC momentum fraction of the gluon. The initial scale Q_0 corresponding to the quark mass regulator m_{col} is set to the quark mass $m_q = 0.26$ GeV encoded in the non-perturbative three-quark BS wavefunction presented at the end of sec. II A. Also, we choose $Q = M_{\text{UV}} = 10m_{\text{col}}$.

The computation of the evolved density matrix is numerically very challenging. It requires the evaluation of a seven dimensional integral, e.g. eq. (35), at each of $N^2 \times N^2/2$ entries of the $(\xi, \eta) - (\xi', \eta')$ symmetric density matrix, where N is the number of bins per variable. We have used the vegas+ v6.2 algorithm [43, 44] to estimate the density matrix with collinear gluon emission corrections. The evolved dPDF, as the diagonal of the density matrix, only requires N^2 integrations, so we have computed it with $N = 100$ bins. On the other hand, studying the effects of the PEN transformation requires the entire density matrix, limiting us to $N = 20$ bins. For this reason we refrain from showing the dPDF to sPDF ratio $C(x_1, x_2)$ but focus instead on the dPDF itself.

Our numerical results are shown in fig. 5. The maximum of the dPDF occurs at $\xi = 1/2$, of course, and near $\eta = 2/3$. The strength of this peak is reduced by the PEN transformation. On the other hand, it enhances the dPDF for asymmetric momentum fractions (small or large ξ) when either one of them is large ($\eta = 2/3 \pm 0.15$). PEN also enhances the dPDF for similar ($\xi = 1/2 \pm 0.15$) but fairly small ($\eta \lesssim 0.3$) momentum fractions. Put the other way: entanglement correlations associated with the negativity tend to suppress the dPDF for small (and similar) as well as for large but strongly asymmetric momentum fractions, but instead strengthen the peak near $x_1 = x_2$ and $x_1 + x_2 = 2/3$. Thus, after evolution to higher Q^2 the strongest effects from quantum correlations appear in a different regime than at the initial scale Q_0^2 ; we recall from sec. II D that for the non-perturbative constituent quark LCwf the strongest effects occurred for rather asymmetric momentum fractions x_1 and x_2 , and well below the kinematic boundary $x_1 + x_2 = 1$.

IV. SUMMARY

The density matrix $\rho_{x_1 x_2, x'_1 x'_2}$ describing the LC momentum distributions of two quarks in the proton is obtained by tracing the pure proton state $|P\rangle \langle P|$ over all unobserved degrees of freedom. This, in general, results in a mixed state with non-zero von Neumann entropy. The purpose of this paper was to apply methods from Quantum Information Theory, specifically the negativity measure, to investigate quantum entanglement correlations of double quark momentum fractions.

⁷ For a single quark flavor, and with the initial gluon PDF set to 0.

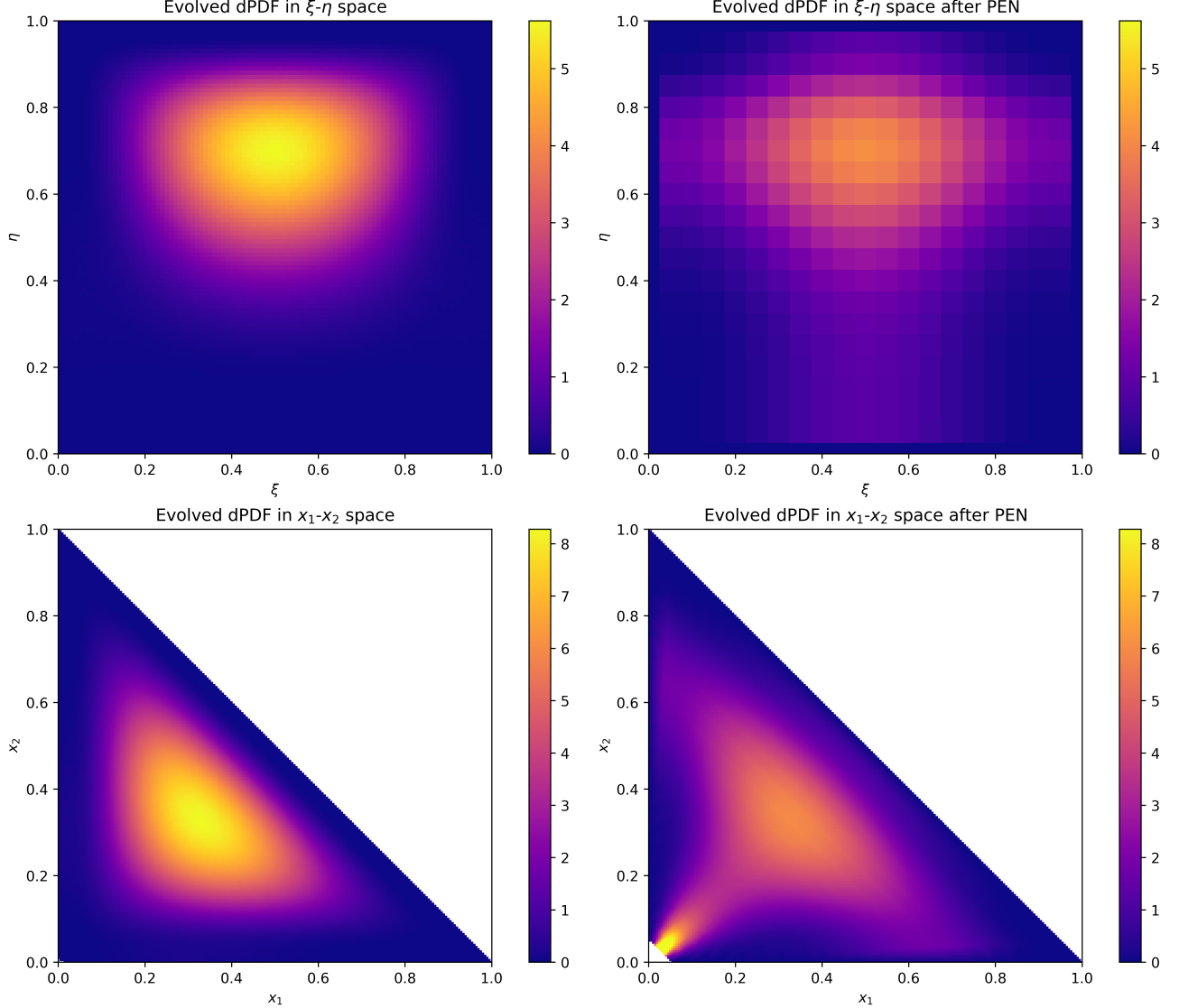


FIG. 5: Contour plots of the dPDF at $Q^2/Q_0^2 = 100$ with $\alpha_s = 0.1$, $x = 0.1$, and $Q_0 = m_q$ as a function of $\eta = x_1 + x_2$ and $\xi = x_1/(x_1 + x_2)$ (top), and x_1 and x_2 (bottom). Left: the dPDF obtained here from the Brodsky-Schlumpf model LCwf with corrections due to collinear gluon emission. Right: same, after the removal of quantum correlations via the PEN transformation.

The diagonal $f_{qq}(x_1, x_2) = \rho_{x_1 x_2, x_1 x_2}$ of the density matrix corresponds to the double quark parton distribution (dPDF). In general the dPDF differs from the product of two single quark PDFs due to correlations. Classical correlations can be encoded in probabilistic mix of product states, i.e. a separable state (4); for such a state the “entanglement negativity” measure of Quantum Information Theory is zero. On the other hand, a non-zero negativity implies the presence of non-separable quantum correlations.

In sec. II we have computed the density matrix over the two-quark LC momentum fractions in an effective LC constituent quark model of the proton intended for not too small $x_i \sim 0.1$ or greater, and a low resolution scale Q_0^2 . (For an improved description of the proton at low scale one should account for non-perturbative contributions from higher Fock states such as $|qqqg\rangle$ and $|qqqq\bar{q}\rangle$ in the future.) Upon purging the density matrix of its entanglement negativity and the associated quantum correlations, we observe strong modifications of the dPDF in some range of momentum fractions, specifically for asymmetric x_1, x_2 far below the bound $x_1 + x_2 = 1$. In fact, in this regime we find that purging the entanglement negativity turns a suppression of the quantum correlated dPDF (relative to a product of two single quark PDFs) into a strong enhancement. On the other hand, for large $x_1 + x_2$ or $x_1 \simeq x_2$ the effect of such quantum correlations in this model is found to be small whereas classical correlations enforce $f_{qq}(x_1, x_2)/f_q(x_1)f_q(x_2) \rightarrow 0$ as $x_1 + x_2 \rightarrow 1$.

In sec. III we derived the corrections to $\rho_{x_1 x_2, x'_1 x'_2}$ due to the emission of one collinear gluon. This corresponds

to one step of QCD scale evolution to $Q^2 > Q_0^2$ of the entire density matrix, assuming $\alpha_s \log Q^2/Q_0^2 \ll 1$; on the diagonal we recover the dPDF DGLAP evolution in terms of convolutions of splitting functions and dPDFs. From the density matrix at the new scale Q^2 we obtain first qualitative predictions for the QCD scale evolution of quantum entanglement in double quark states in the proton. These results are qualitative because we do not resum multiple evolution steps and are therefore limited to unrealistically weak coupling, $\alpha_s = 0.1$, and large cutoff on the LC momentum of the gluon, $x = 0.1$. Even so, interestingly, at the higher scale we do observe significant effects due to quantum correlations for nearly symmetric momentum fractions, $x_1 \simeq x_2$, for fairly small $x_1 + x_2 \lesssim 0.3$, where their effect is to suppress the dPDF. These initial explorations motivate the development of the complete QCD evolution equations of the full two-quark density matrix, to account for the emission of an entire ladder of partons. This work is in progress.

V. ACKNOWLEDGEMENTS

We acknowledge support by the DOE Office of Nuclear Physics through Grant DE-SC0002307.

[1] V. L. Korotkikh and A. M. Snigirev, Double parton correlations versus factorized distributions, *Phys. Lett. B* **594**, 171 (2004), [arXiv:hep-ph/0404155](https://arxiv.org/abs/hep-ph/0404155).

[2] J. R. Gaunt and W. J. Stirling, Double Parton Distributions Incorporating Perturbative QCD Evolution and Momentum and Quark Number Sum Rules, *JHEP* **03**, 005, [arXiv:0910.4347 \[hep-ph\]](https://arxiv.org/abs/0910.4347).

[3] B. Blok, Y. Dokshitzer, L. Frankfurt, and M. Strikman, The Four jet production at LHC and Tevatron in QCD, *Phys. Rev. D* **83**, 071501 (2011), [arXiv:1009.2714 \[hep-ph\]](https://arxiv.org/abs/1009.2714).

[4] M. Diehl, D. Ostermeier, and A. Schafer, Elements of a theory for multiparton interactions in QCD, *JHEP* **03**, 089, [Erratum: JHEP 03, 001 (2016)], [arXiv:1111.0910 \[hep-ph\]](https://arxiv.org/abs/1111.0910).

[5] M. Diehl and J. R. Gaunt, Double parton scattering theory overview, *Adv. Ser. Direct. High Energy Phys.* **29**, 7 (2018), [arXiv:1710.04408 \[hep-ph\]](https://arxiv.org/abs/1710.04408).

[6] M. Jaarsma, R. Rahn, and W. J. Waalewijn, Towards double parton distributions from first principles using Large Momentum Effective Theory, *JHEP* **12**, 014, [arXiv:2305.09716 \[hep-ph\]](https://arxiv.org/abs/2305.09716).

[7] W. Broniowski and E. R. Arriola, Valence double parton distributions of the nucleon in a simple model, *Few-Body Syst* **55**, 381 (2014), [arXiv:1310.8419 \[hep-ph\]](https://arxiv.org/abs/1310.8419).

[8] K. Golec-Biernat and E. Lewandowska, How to impose initial conditions for QCD evolution of double parton distributions?, *Phys. Rev. D* **90**, 014032 (2014), [arXiv:1402.4079 \[hep-ph\]](https://arxiv.org/abs/1402.4079).

[9] N. Armesto, F. Dominguez, A. Kovner, M. Lublinsky, and V. Skokov, The Color Glass Condensate density matrix: Lindblad evolution, entanglement entropy and Wigner functional, *JHEP* **05**, 025, [arXiv:1901.08080 \[hep-ph\]](https://arxiv.org/abs/1901.08080).

[10] K. Golec-Biernat, E. Lewandowska, M. Serino, Z. Snyder, and A. M. Stasto, Constraining the double gluon distribution by the single gluon distribution, *Phys. Lett. B* **750**, 559 (2015), [arXiv:1507.08583 \[hep-ph\]](https://arxiv.org/abs/1507.08583).

[11] H.-M. Chang, A. V. Manohar, and W. J. Waalewijn, Double Parton Correlations in the Bag Model, *Phys. Rev. D* **87**, 034009 (2013), [arXiv:1211.3132 \[hep-ph\]](https://arxiv.org/abs/1211.3132).

[12] M. Rinaldi, S. Scopetta, M. Traini, and V. Vento, Double parton correlations and constituent quark models: a Light Front approach to the valence sector, *JHEP* **12**, 028, [arXiv:1409.1500 \[hep-ph\]](https://arxiv.org/abs/1409.1500).

[13] M. Rinaldi and F. A. Ceccopieri, Relativistic effects in model calculations of double parton distribution function, *Phys. Rev. D* **95**, 034040 (2017), [arXiv:1611.04793 \[hep-ph\]](https://arxiv.org/abs/1611.04793).

[14] M. Rinaldi, S. Scopetta, M. C. Traini, and V. Vento, Correlations in Double Parton Distributions: Perturbative and Non-Perturbative effects, *JHEP* **10**, 063, [arXiv:1608.02521 \[hep-ph\]](https://arxiv.org/abs/1608.02521).

[15] D. Reitinger, C. Zimmermann, M. Diehl, and A. Schäfer, Double parton distributions with flavor interference from lattice QCD, *JHEP* **04**, 087, [arXiv:2401.14855 \[hep-lat\]](https://arxiv.org/abs/2401.14855).

[16] D. E. Kharzeev and E. M. Levin, Deep inelastic scattering as a probe of entanglement, *Phys. Rev. D* **95**, 114008 (2017), [arXiv:1702.03489 \[hep-ph\]](https://arxiv.org/abs/1702.03489).

[17] D. E. Kharzeev, Quantum information approach to high energy interactions, *Phil. Trans. A. Math. Phys. Eng. Sci.* **380**, 20210063 (2021), [arXiv:2108.08792 \[hep-ph\]](https://arxiv.org/abs/2108.08792).

[18] D. E. Kharzeev and E. Levin, Deep inelastic scattering as a probe of entanglement: Confronting experimental data, *Phys. Rev. D* **104**, L031503 (2021), [arXiv:2102.09773 \[hep-ph\]](https://arxiv.org/abs/2102.09773).

[19] A. Kovner and M. Lublinsky, Entanglement entropy and entropy production in the Color Glass Condensate framework, *Phys. Rev. D* **92**, 034016 (2015), [arXiv:1506.05394 \[hep-ph\]](https://arxiv.org/abs/1506.05394).

[20] A. Kovner, M. Lublinsky, and M. Serino, Entanglement entropy, entropy production and time evolution in high energy QCD, *Phys. Lett. B* **792**, 4 (2019), [arXiv:1806.01089 \[hep-ph\]](https://arxiv.org/abs/1806.01089).

[21] H. Duan, A. Kovner, and V. V. Skokov, Gluon quasiparticles and the CGC density matrix, *Phys. Rev. D* **105**, 056009 (2022), [arXiv:2111.06475 \[hep-ph\]](https://arxiv.org/abs/2111.06475).

[22] A. Dumitru, A. Kovner, and V. V. Skokov, Entanglement entropy of the proton in coordinate space, *Phys. Rev. D* **108**, 014014 (2023), [arXiv:2304.08564 \[hep-ph\]](https://arxiv.org/abs/2304.08564).

- [23] M. Hentschinski, D. E. Kharzeev, K. Kutak, and Z. Tu, QCD evolution of entanglement entropy, *Rept. Prog. Phys.* **87**, 120501 (2024), arXiv:2408.01259 [hep-ph].
- [24] Y. Hatta and J. Montgomery, Maximally entangled gluons for any x , (2024), arXiv:2410.16082 [hep-ph].
- [25] S. Bhattacharya, R. Boussarie, and Y. Hatta, Spin-orbit entanglement in the Color Glass Condensate, *Phys. Lett. B* **859**, 139134 (2024), arXiv:2404.04208 [hep-ph].
- [26] L. Gurvits, Classical deterministic complexity of Edmonds' Problem and quantum entanglement, in *35th annual ACM symposium on Theory of computing* (2003).
- [27] S. Gharibian, Strong NP-hardness of the quantum separability problem, *Quant. Inf. Comput.* **10**, 0343 (2010), arXiv:0810.4507 [quant-ph].
- [28] O. Ghne and G. Tth, Entanglement detection, *Phys. Rept.* **474**, 1 (2009), arXiv:0811.2803 [quant-ph].
- [29] R. Horodecki, P. Horodecki, M. Horodecki, and K. Horodecki, Quantum entanglement, *Rev. Mod. Phys.* **81**, 865 (2009), arXiv:quant-ph/0702225.
- [30] D. Chruscinski and G. Sarbicki, Entanglement witnesses: construction, analysis and classification, *J. Phys. A* **47**, 483001 (2014), arXiv:1402.2413 [quant-ph].
- [31] M. J. Donald, M. Horodecki, and O. Rudolph, The uniqueness theorem for entanglement measures, *Journal of Mathematical Physics* **43**, 4252–4272 (2002).
- [32] A. Peres, Separability Criterion for Density Matrices, *Phys. Rev. Lett.* **77**, 1413 (1996), arXiv:quant-ph/9604005 [quant-ph].
- [33] M. Horodecki, P. Horodecki, and R. Horodecki, Separability of mixed states: necessary and sufficient conditions, *Phys. Lett. A* **233**, 1 (1996), arXiv:quant-ph/9605038 [quant-ph].
- [34] M. M. Wilde, From Classical to Quantum Shannon Theory 10.1017/9781316809976.001 (2011), arXiv:1106.1445 [quant-ph].
- [35] F. Schlumpf, Relativistic constituent quark model of electroweak properties of baryons, *Phys. Rev. D* **47**, 4114 (1993), [Erratum: Phys. Rev. D 49, 6246 (1994)], arXiv:hep-ph/9212250.
- [36] S. J. Brodsky and F. Schlumpf, Wave function independent relations between the nucleon axial coupling g_A and the nucleon magnetic moments, *Phys. Lett. B* **329**, 111 (1994), arXiv:hep-ph/9402214.
- [37] B. L. G. Bakker, L. A. Kondratyuk, and M. V. Terentev, On the formulation of two-body and three-body relativistic equations employing light front dynamics, *Nucl. Phys. B* **158**, 497 (1979).
- [38] C. Qian, S. Xu, Y.-G. Yang, and X. Zhao, Quark and gluon entanglement in the proton based on a light-front Hamiltonian, (2024), arXiv:2412.11860 [hep-ph].
- [39] A. Dumitru and E. Kolbusz, Quark pair angular correlations in the proton: Entropy versus entanglement negativity, *Phys. Rev. D* **108**, 034011 (2023), arXiv:2303.07408 [hep-ph].
- [40] G. Dahl, J. Leinaas, J. Myrheim, and E. Ovrum, A tensor product matrix approximation problem in quantum physics, *Linear Algebra and its Applications* **420**, 711 (2007).
- [41] A. Dumitru and E. Kolbusz, Quark and gluon entanglement in the proton on the light cone at intermediate x , *Phys. Rev. D* **105**, 074030 (2022), arXiv:2202.01803 [hep-ph].
- [42] A. Dumitru and R. Paatelainen, Sub-femtometer scale color charge fluctuations in a proton made of three quarks and a gluon, *Phys. Rev. D* **103**, 034026 (2021), arXiv:2010.11245 [hep-ph].
- [43] G. P. Lepage, Adaptive multidimensional integration: VEGAS enhanced, *J. Comput. Phys.* **439**, 110386 (2021), arXiv:2009.05112 [physics.comp-ph].
- [44] G. P. Lepage, vegas 6.2 – project description, <https://pypi.org/project/vegas/> (2013).